Bima Journal of Science and Technology, Vol. 8(4A) Dec, 2024 ISSN: 2536-6041

DOI: 10.56892/bima.v8i4.1151

Orange Peel-Mediated Synthesis of Fe_3O_4 Nanoparticles for the Removal of Ibuprofen from Domestic Wastewater

H. I Adamu[1], M.A Richard[1], A.O Olaniyi[2]

Department of Environmental Management, Kaduna State University Kaduna

Corresponding Authors: habibadamu99@kasu.edu.ng

ABSTRACT

This study explores the eco-friendly production of iron oxide nanoparticles utilizing oranges orange peel extract, focusing on their characterization and application in removing ibuprofen from domestic wastewater. The study investigated the adsorption of ibuprofen onto the nanoparticles under various conditions, encompassing pH levels, starting adsorbate concentration, duration of contact, amount of adsorbent, and temperature. In-depth analysis of the adsorption data using diverse isotherm and kinetic models provided valuable insights into the mechanisms and parameters involved. Characterization revealed that the nanoparticles display a nanocrystalline structure with a cubic shape, high surface area, and are primarily composed of iron (Fe) and oxygen (O). They possess a Z-average of 42.60, feature a Fe-O bond at 693.30 cm^{-1}, and show UV-Visible absorbance at 285 nm. Batch adsorption experiments demonstrated that the removal efficiency improved with increased adsorbent doses (20-100 mg), reaching a peak efficiency of 80.15% at 100 mg. However, the adsorptive capacity diminished as the temperature rose above room temperature, and the initial adsorbate concentration showed an inconsistent pattern with the optimum adsorption at 10 mg/L and contact time of 15 min and a pH of 7. The adsorption process conformed to a pseudo-second-order model. (R^2=0.92174), indicating a reliance on active sites and ibuprofen concentration, suggesting chemisorption mechanisms. The Langmuir isotherm model best aligned with the data (R^2=0.93461), indicating monolayer coverage on nanoparticles with a strong affinity for ibuprofen. Thermodynamic analysis verified that the adsorption occurred spontaneously (negative ΔG) and exothermic (negative ΔH), consistent with decreased capacity at elevated temperatures. This study demonstrates the efficiency of iron oxide nanoparticles (IONPs) in reducing ibuprofen levels in domestic wastewater, with consistent reduction percentages ((1.30-0.0544 mg/L) highlighting the method's reliability and scalability for treating pharmaceutical contaminants across various environmental settings.

Keywords: Orange peel, Nanoparticles, Ibuprofen, Wastewater and Adsorption

INTRODUCTION

Pharmaceutical contaminants in water bodies have become a significant environmental concern, with ibuprofen a commonly used non-steroidal anti-inflammatory drug (NSAID) frequently detected in hospital and household wastewater. The environmental effects of ibuprofen are complex, as it can interfere with the endocrine systems of aquatic life, causing reproductive and developmental problems (Batucan *et al*., 2022). Moreover, ibuprofen's presence in water can lead to the emergence of antibiotic-resistant bacteria, adding to public health challenges (Muñiz-González, 2021). Conventional wastewater treatment methods, like activated sludge processes, often fail to fully eliminate pharmaceutical contaminants such as ibuprofen. This inadequacy necessitates the exploration of more effective and sustainable removal techniques (Katare *et al*., 2023).

DOI: 10.56892/bima.v8i4.1151

The challenge of removing ibuprofen from wastewater is compounded by its chemical stability and low biodegradability. Conventional treatment methods, including biological degradation and chemical oxidation, often fall short in achieving complete removal. Adsorption has become a promising method for removing pharmaceutical contaminants due to its straightforwardness, effectiveness, and affordability. Adsorbents like activated carbon, zeolites, and various metal oxides have been widely researched for this purpose (Brillas, 2022).

Nonetheless, the quest for more efficient, sustainable, and cost-effective adsorbents continues. Recently, nanoparticles have gained attention because of their large surface area and unique physicochemical properties, which improve their adsorption capabilities. Iron oxide nanoparticles, in particular, have shown significant potential for adsorbing various contaminants, including pharmaceuticals (Zubair *et al*., 2023). Synthesizing iron oxide nanoparticles using green methods, such as plant extracts, offers an eco-friendly and sustainable approach. Orange peel, a commonly available agricultural byproduct, is rich in bioactive compounds that act as reducing and stabilizing agents in nanoparticle synthesis. (Usman *et al*., 2024). Using orange peel extract to synthesize iron oxide nanoparticles not only provides an eco-friendly approach but also enhances the value of agricultural waste (Govidarajan *et al*., 2023).

Therefore, this study seeks to examine the effectiveness of iron oxide nanoparticles, synthesized using orange peel extract, in adsorbing and removing ibuprofen from household wastewater.

MATERIALS AND METHODS

Sample Collection

Collection of orange peel sample

The orange peel sample was collected from the nearby fruit market in Bakin Dogo, located within the Kaduna Metropolis Kaduna State, Nigeria. These samples were carefully placed in labeled polythene bags and taken to the laboratory, then carefully washed with distilled water to remove impurities, the peels were cut into smaller pieces and then dried in the shade for seven days and finely ground in an electric blender (Silver Crest) to obtain a powdered form and sieved through a 60 mm mesh (Mohamed Khalith *et al*., 2022).

Collection of domestic wastewater sample

The domestic wastewater samples were collected from three distinct zones within the Kaduna metropolis, chosen based on each area's population size. Sample A, obtained from the low-density populated Malali/Unguwar Rimi GRA, Sample B, collected from the middle-density populated Kawo/Unguwar Dosa area, and Sample C, taken from the high population density Badiko/hayin danmani locale. These samples were acquired using clean 1-liter glass bottles from various points along the drainage systems within the study areas at three separate intervals. Subsequently, they were carefully transported to the laboratory in an ice bath container for analysis.

Preparation of Orange Peel Extract

Orange peel powder (10 mg) was precisely weighed using an analytical balance and transferred to an Erlenmeyer flask. Polyphenol extraction was performed using 150 mL of distilled water at 40°C for 2 hours, with constant stirring at 500 rpm, following a modified protocol from Faisal *et al*. (2021). The resulting extract's polyphenol content was then quantified using the Folin-Ciocalteu assay method, as described by Kupina *et al*. (2018)

DOI: 10.56892/bima.v8i4.1151

Synthesis of Iron Oxide Nanoparticles

Iron oxide nanoparticles were synthesized using a coprecipitation approach. Orange peel extract (100 mL) was added to an Erlenmeyer flask on a magnetic stirrer. A solution of Fe^{3+} and Fe^{2+} salts (2:1 molar ratio, 50 mL) was slowly added, and the pH adjusted from 6.3 to 11 with 1M NaOH. Stirring continued for 1 hour to facilitate reaction completion.

After centrifugation at 5000 rpm for 10 minutes, the nanoparticles were subjected to a series of washing steps, comprising five cycles with deionized water and a final ethanol rinse to remove impurities. The nanoparticles were then oven-dried at 130°C and stored in an airtight container. The formation of nanoparticles was indicated by a visible color change, which was further confirmed using UV-vis spectroscopy, as described by Abdullaeva (2017).

Characterization of the Synthesized Iron Oxide (Fe_3O_4) Nanoparticles

The functional groups present in the orange peel extract and iron oxide nanoparticles (IONPs) were characterized using Fourier Transform Infrared Spectroscopy (FTIR) on a Shimadzu FTIR 8400 S spectrophotometer, covering a spectral range of 4000-400 cm^{-1}. The conversion of iron ions to iron oxide nanoparticles was monitored using UV-Visible absorption spectroscopy on a T70 PG Instruments spectrophotometer, operating within a range of 200-800 nm.

The size of the synthesized metal nanoparticles was measured using dynamic light scattering on a Malvern Panalytical Zetasizer Nano ZS90, following the ASTM E11:61 standard test method (ASTM Standard Test Method (E11-17) 2017), as described by Abdulaeva (2017).

Scanning electron microscopy (SEM) on a JOEL JSM 7600F microscope equipped with Energy-Dispersive Spectroscopy (EDS) was used to analyse the surface morphology and elemental composition. The crystal structure and material composition were analyzed with X-Ray Diffraction (XRD) on a Rigaku MiniFlex 6G machine. Additionally, a JW-DA: 76502057en China surface area analyzer was used to determine the surface area.

Batch Adsorption Experiment

The removal of ibuprofen was studied by batch experiments, adapting methods from Ahmadpour *et al*. (2019). To optimize adsorbent dosage, amounts ranging from 20 to 100 mg were tested. pH levels were adjusted to 3, 5, 7, 9, and 11 using 0.1 M HCl and NaOH. The adsorbate concentration was varied between 2 and 10 mg/L, and adsorption kinetics were monitored over 5 to 40 minutes at 200 rpm. Temperature effects were analyzed between 27-42°C (300-320K) in 5°C increments under optimized conditions, with constant shaking at 200 rpm.

The residual ibuprofen was determined using UV-Visible spectroscopy (PerkinElmer Operetta Microplate reader with Cermax Xenon Fiber-Optic Light Source, Model XL3000) at a wavelength of 222nm and extrapolated from a prepared calibration curve.

The definite quantity of ibuprofen remove under different experimental conditions was determined using the following equation.

$$qe = \frac{(Co-Ce)V}{W} \quad (1)$$

$$\%\ Removal = \frac{Co-Ce}{Co} * 100 \quad (2)$$

In this equation, q_e denotes the equilibrium adsorption capacity of ibuprofen onto the iron oxide nanoparticles (IONPs), expressed in milligrams of ibuprofen per gram of IONPs (mg/g). The variables C_o and C_e represent the initial and equilibrium concentrations of ibuprofen in the aqueous solution, respectively,

DOI: 10.56892/bima.v8i4.1151

measured in milligrams per liter (mg/L). Additionally, V and W signify the volume of the aqueous solution (in milliliters, mL) and the mass of IONPs used for adsorption (in grams, g), respectively.

Determination of Point of Zero Charge (pH_{PZC})

The method described by Bakatula *et al*., (2018) was used to study the pH point of zero charge (PZC) of the IONPs employing the salt addition method. Equal quantities of IONPs (0.2g) were added to various solutions containing 0.1 M $NaNO_3$, with pH levels ranging from 2 to 11 (±0.1 pH units). The pH was adjusted as needed using 0.1 M HNO_3 and 0.1 M NaOH to reach the desired values. Subsequently, the samples underwent agitation for 24 hours at 200 rpm using a rotary agitator. Following sedimentation, the pH values of the liquid above the sediment in each tube were gauged and recorded as pH_f. The PZC was determined by plotting ΔpH (=pH_f – pH_i) against pH_i.

Thermodynamic Study for the Adsorption of Ibuprofen Using the Synthesized IONPs

The thermodynamic parameters were derived from the study results on how temperature affects the adsorption of ibuprofen.

The three essential parameters of the thermodynamic study which are the Gibbs free energy (ΔG^o), enthalpy change (ΔH^o) and change in entropy (ΔS^o) were investigated using the Van't Hoff equation. The Gibbs free energy (ΔG^o),) is expressed as;

$$\Delta G = -RT\ln K_o \quad (3)$$

And

$$K_o = q_e/C_e \quad (4)$$

Here, (R), (T), and (K_o) represent the molar gas constant (8.314 J/Kmol), absolute temperature (K), and the thermodynamic constant (dimensionless), respectively. The third principle of thermodynamics describes the relationship between (ΔG^o), (ΔH^o) and (ΔS^o) in the equation.

$$\Delta G^o = \Delta H^o - T\Delta S^o \quad (5)$$

Here, ΔG^o, ΔH^o and ΔS^o are the Gibbs free energy (J mol^{-1}), enthalpy change (J mol^{-1}), and entropy change (J mol^{-1} K^{-1}) respectively. By combining equations 4 and 5, the Van't Hoff equation is formulated, as shown in equation 6.

$$\ln K_o = -\frac{-\Delta H^o}{RT} + \frac{\Delta S^o}{R} \quad (6)$$

Hence, ΔG^O, ΔH^o and ΔS^o can be derived from the slope and intercept of the graph of $\ln K_o$ on the y axis and 1/T on the x axis produce a straight line with the slope and intercept being $-\Delta H^o/R$ and $\Delta S^o/R$ respectively.

Determination of the Concentration of Ibuprofen from Domestic Wastewater and its Removal with the Synthesized IONPs

The amount of ibuprofen was determined in the collected wastewater samples using micro plate reader. A 250 µL of the sample was measured using a micropipette and transferred to a clean micro plate in triplicate and analyze at a wavelength of 222 nm for the ibuprofen respectively. The concentration of ibuprofen was calculated from the calibration curve (Babtista *et al*., 2021).

The removal of ibuprofen from domestic wastewater was investigated using a batch experiment technique. A 50 mL sample of wastewater was measured into a 100 mL Erlenmeyer flask. The adsorption parameters were set as follows: 100 mg of adsorbent dosage, pH 7 (adjusted using 0.1 M HCl and 0.1 M NaOH). The mixture was agitated at 200 rpm for 15 minutes at room temperature. The residual concentration of the ibuprofen was determined after from a calibration curve.

DOI: 10.56892/bima.v8i4.1151

Kinetic Studies

Under optimal conditions, adsorption kinetics data were analyzed using pseudo-first order, pseudo-second order, intraparticle diffusion, and Elovich models to determine the adsorption order and mechanism, with regression values assessing model applicability. (Plazinski, et *al*., 2013).

The pseudo-first order kinetic model was analyzed using the integrated rate law equation.

$$\ln (q_e - q_t) = lnq_e - k_i t \qquad (7)$$

In this context, q_e and q_t (both expressed in mg/g) denote the equilibrium adsorption capacity and the amount of adsorbate adsorbed at time t, respectively. To determine the adsorption rate constant (K_1) for ibuprofen sorption, a linear plot of $\ln(q_e - q_t)$ versus time (t) will be plotted, and the slope of this plot will be used to calculate K_1.

The integrated rate law equation for the pseudo-second order kinetic model is:

$$\frac{t}{qt} = \frac{1}{K_2 q_e^2} + \frac{1}{q_e} \qquad (8)$$

In this study, qe and q_t (both expressed in mg/g) represent the equilibrium adsorption capacity and the amount of ibuprofen adsorbed per unit mass of adsorbent at time t, respectively. The pseudo-first-order rate constant (k') can be calculated from the slope of a linear plot of t/q_t versus t, where (t) represents time (in seconds or minutes) and q_t represents the amount of ibuprofen adsorbed per unit mass of adsorbent at time t (in mg/g).

The equation for the intraparticle diffusion kinetic model is:

$$q_t = k_p t^{1/2} + C \qquad (9)$$

Here, (q_t) represents the amount of adsorbate per unit mass of adsorbent at time (t) (mg/g), (k_p) is the interparticle diffusion rate constant (mg/g $min^{1/2}$)), (t) is the time (minutes), and (C) is the intercept (mg/g), which indicates the boundary layer effect. The value of k_p indicates the rate of interparticle diffusion. The higher the value of k_p, the faster the interparticle diffusion. The value of C indicates the boundary layer effect. A larger value of (C) signifies a stronger boundary layer effect (Kajjumba *et al*., 2018).

The data was graphed as (q_t) against ($t^{1/2}$), resulting in a straight line as per the intraparticle diffusion kinetic model equation.

The Elovich kinetic model equation is given by:

$$q_t = \frac{1}{\beta}\ln(\alpha\beta) + \frac{1}{\beta} lnt \qquad (10)$$

Here, (q_t) is the amount of adsorbate per unit mass of adsorbent at time (t) (mg/g), (α) represents the initial adsorption rate (mg/g min), (β) is the desorption constant (g/mg), and (t) is the time (minutes). The value of (α) reflects the initial speed of the adsorption process. The higher the value of α, the faster the adsorption. A greater value of (α) signifies a quicker adsorption process. The value of () reflects the level of surface heterogeneity, with a higher (β) indicating a more heterogeneous surface (Plazinski, *et al*., 2013).

To apply the Elovich kinetic model, the experimental data of adsorbate amount per unit mass of adsorbent over time was utilized. The data was plotted as (q_t) against (lnt), resulting in a straight line according to the Elovich kinetic model equation. Linear regression analysis can be conducted to determine the slope and intercept of the plot, which correspond to (1/β) and (1/ β ln (αβ), respectively. The values of (α) and (β) can be derived from the intercept and slope. The coefficient of determination (R^2) can be used to assess the fit quality.

Adsorption Isotherm

DOI: 10.56892/bima.v8i4.1151

To elucidate the adsorption mechanism and determine key adsorption parameters, the experimental data will be analyzed using three prominent isotherm models: Langmuir, Freundlich, and Temkin. The Langmuir isotherm equation, which assumes monolayer adsorption on a homogeneous surface, will be employed to investigate the adsorption process and estimate relevant parameters.

The Langmuir isotherm equation, which indicates monolayer adsorption on a surface (Alfonso *et al*., 2016), is presented below.

$$q_e = \frac{q_m K_L C_e}{1+K_L C_e} \quad (11)$$

The Langmuir isotherm was converted into its linear form, as shown in Equation (12), to identify the adsorption parameters.

$$\frac{1}{q_e} = \frac{1}{K_L q_{maz}} . \frac{1}{C_e} + \frac{1}{q_{max}} \quad (12)$$

In this context, the following parameters are defined: K_L, the Langmuir constant (L/mg), which characterizes the adsorption energy; q_{max}, the maximum adsorption capacity (mg/g), representing the highest amount of pharmaceutical that can be adsorbed per gram of adsorbent at equilibrium; and C_e, the equilibrium concentration (mg/L) of the adsorbate in the solution.

Plotting the experimental data of 1/qe versus $1/C_e$ yields a linear relationship, characterized by a slope of 1/ ($q_{max}K_L$) and an intercept of $1/q_{max}K_L$. From this linear plot, the values of q_{max} and K_L can be readily extracted from the slope and intercept, respectively. The goodness of fit is evaluated using the coefficient of determination (R_2), where values approaching 1 signify an excellent fit, indicating that the Langmuir model accurately describes the adsorption process.

The Langmuir isotherm's essential characteristics are encapsulated in a dimensionless constant, the separation factor (R_L), which plays a crucial role in predicting the adsorption process's efficiency (Alfonso *et al*., 2016). This factor can be calculated using the following equation, enabling the evaluation of the adsorption process's feasibility and potential performance.

$$R_L = \frac{1}{1+K_L C_0} \quad (13)$$

In this context, K_L represents the Langmuir constant (mg/L), and Co denotes the initial concentration of the adsorbate (mg/L). The dimensionless separation factor (R_L) indicates the adsorption feasibility: unfavorable adsorption occurs when $R_L > 1$, linear adsorption when $R_L = 1$, favorable adsorption when $0 < R_L < 1$, and irreversible adsorption when $R_L = 0$.

The Freundlich isotherm equation, indicating that adsorption takes place on a heterogeneous surface (Alfonso *et al*., 2016), is presented as follows.

$$log q_e = \log K_F + \frac{1}{n} log C_e \quad (14)$$

Here, (K_F) and (n) are the isotherm constants representing the adsorption capacity and intensity, while (1/n) reflects the adsorption strength.

Plotting the experimental data of log (q_e) versus log (C_e) yields a linear relationship, characterized by a slope of 1/n and an intercept of ln(K_F). The Freundlich constants, K_F and n, can be readily determined from the intercept and slope, respectively. The goodness of fit is assessed by the coefficient of determination (R_2), where values approaching 1 indicate a more accurate representation of the data.

The Temkin isotherm model takes into account the effects of indirect interactions between adsorbate molecules on the adsorption process. This model assumes a linear decrease in the heat of adsorption (DH_{ads}) for all molecules in the layer as surface coverage increases (N'diaye *et al*., 2020).

DOI: 10.56892/bima.v8i4.1151

The linear form of Temkin isotherm model is given by the following

$$\ln(q_e) = \ln(a) + \frac{RT}{b}\ln(C_e) \qquad (15)$$

By plotting the experimental data of ($\ln(q_e)$) against ($\ln(C_e)$), a straight line is formed with a slope of (RT/b) and an intercept of ($\ln(a)$). The values of "a" and "b" can be derived from the intercept and slope, respectively. The coefficient of determination (R^2) assesses the fit's quality, with values closer to 1 indicating a better fit.

RESULTS AND DISCUSSION

Polyphenol Contents and FTIR Characterization of the Orange Peel Extract

The Folin-Ciocalteu assay indicates a high polyphenol content in the orange peel extract, with a gallic acid equivalent value of 33.40 mg/g. This abundance of polyphenolic compounds significantly contributes to the nanoparticle synthesis, enabling the efficient reduction of iron ions and subsequent formation of iron oxide nanoparticles. Moreover, they provide enhanced protection against oxidation and degradation. The extract's antioxidant properties also contribute to the improved stability and longevity of the nanoparticles, thereby broadening their potential applications (Abdullah *et al*., 2022).

The FTIR spectroscopic analysis of the orange peel extract reveals a complex molecular structure, characterized by distinct absorption peaks (Figure 1). A prominent peak at 1148 cm^{-1} is indicative of ether linkages, which can facilitate the reduction of iron ions and stabilize the resulting nanoparticles through electron donation. Additionally, the presence of hydroxyl groups in phenolic and alcoholic compounds is evidenced by peaks at 1341.90 cm^{-1} and 1080.90 cm^{-1}, respectively. These functional groups play a crucial role in the green synthesis of iron oxide nanoparticles by reducing iron ions and promoting nanoparticle formation (Nawaz *et al*., 2023).

The peak at 3287.50 cm^{-1} indicates the presence of carboxylic acid functional groups, which play a crucial role in the bioreduction of iron ions (Fe^{3+}) to form iron oxide nanoparticles (Fe_2O_3). This process involves the reduction of metal ions by biomolecules, with functional groups like -COOH, O-H, C-O-C, C=C, and -CHO facilitating the reduction (Ishak *et al*., 2019). Carboxylic acid also acts as a capping agent, forming a protective layer around the nanoparticles through biofunctionalization, stabilizing them in aqueous solutions (Jeevanandam *et al*., 2022).

The orange peel extract is rich in phenolic compounds, including flavonoids, phenolic acids, and limonoids, which are known for their various biological activities (Shehata *et al*., 2021). These compounds contribute to the synthesis and stabilization of iron oxide nanoparticles, making the orange peel extract a valuable resource for eco-friendly nanoparticle production.

Characterization of the Synthesized Iron Oxide Nanoparticles

The resulting spectrum of the UV- visible spectroscopy displayed a distinct absorption peak at 285 nm (Figure 2), suggesting the formation of small, nanocrystalline structures with low electron excitation energy. The relationship between nanoparticle size, shape, and optical properties was evident, with smaller particles typically exhibiting increased band gap energies and absorption peaks. Furthermore, the shape of the nanoparticles influenced electron distribution and density of states in the valence and conduction bands, as reported in previous studies (Alangari *et al*., 2022; Nawaz *et al*., 2023).

Plant-derived iron oxide nanoparticles exhibit unique UV-Visible absorption profiles based on their botanical origin and synthesis

DOI: 10.56892/bima.v8i4.1151

conditions. For instance, nanoparticles from *Murraya koenigii* and *Avicennia marina* extracts absorb at 277 nm and 295-301 nm, respectively (Karpagavinayagam and Vedhi, 2019) which indicate the surface plasmon resonance of the iron oxide nanoparticles.

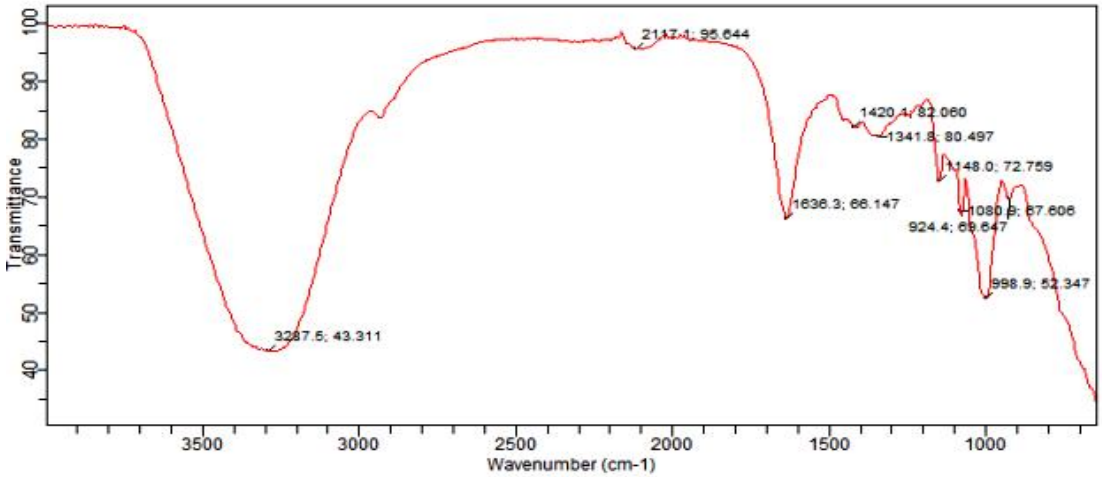

Figure 1: FTIR spectrum of orange peel extract

Surface plasmon resonance (SPR) is a phenomenon where conduction electrons on metal nanoparticles oscillate in resonance with incident light, leading to strong light absorption at specific wavelengths. The SPR wavelength is highly dependent on the size, shape, and material of the nanoparticles, as well as the surrounding medium (Kumari *et al*., 2024).

In this study, iron oxide nanoparticles were synthesized from orange peel extract. The observed SPR at 285 nm suggests that the nanoparticles are relatively small in size. This is consistent with the general trend that smaller nanoparticles exhibit SPR at shorter wavelengths, while larger nanoparticles resonate at longer wavelengths (Sithara *et al*., 2024).

The size-dependent optical properties of iron oxide nanoparticles are influenced by their size, shape, and material, as well as the surrounding medium (Dalal *et al*., 2019). The observed SPR at 285 nm indicates that the nanoparticles are likely to be in the range of a few nanometers to tens of nanometers in size. This is consistent with literature findings, where iron oxide nanoparticles with sizes around 10-50 nm typically show SPR in the UV-visible range (Dadfar *et al*., 2020).

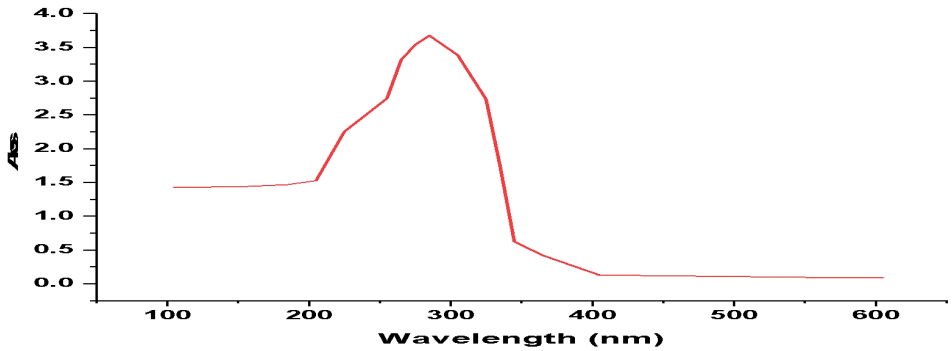

Bima Journal of Science and Technology, Vol. 8(4A) Dec, 2024 ISSN: 2536-6041

DOI: 10.56892/bima.v8i4.1151

Figure 2: UV-Visible spectra of the iron oxide nanoparticles

Orange peel extract-derived nanoparticles display a heterogeneous size distribution, with a Z average of 42.60 nm and PDI of 0.547 (Figure 3 and 4). The Z-average diameter represents the intensity-weighted mean hydrodynamic size, indicating an average particle size of approximately 42.60 nm. The PDI is a measure of the broadness of the size distribution, with a value of 0.547 suggesting significant variability in particle sizes within the sample. The varying polyphenol content in plant extracts influences nanoparticle size distribution (Jadoun *et al*., 2021). Factors like solvent refractive index, dispersant characteristics, and synthesis method also impact nanoparticle size and polydispersity (Guo *et al*., 2021).

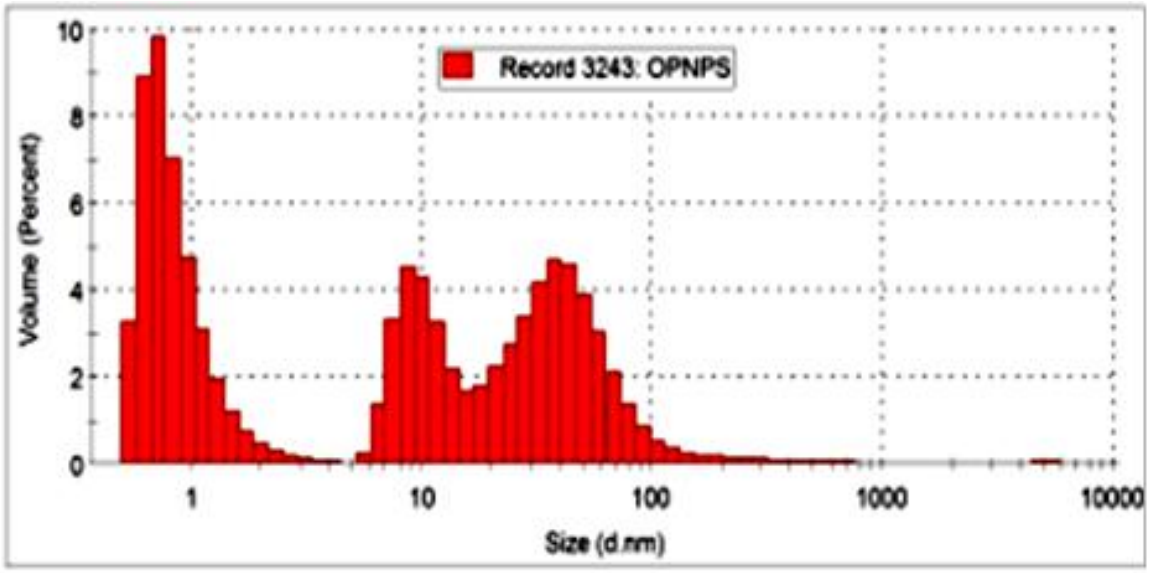

Figure 3: Size distribution of iron oxide nanoparticles against volume.

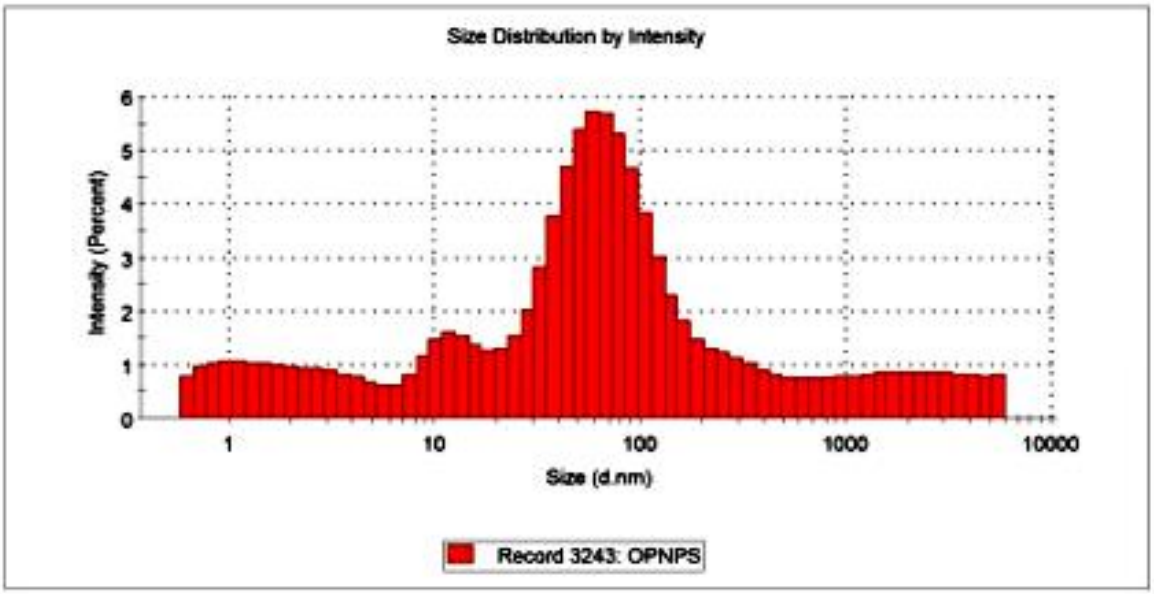

DOI: 10.56892/bima.v8i4.1151

Figure 4: Size distribution of the iron oxide nanoparticles against intensity.

FTIR spectroscopy of IONPs derived from orange peel extract revealed a complex molecular fingerprint, featuring eight prominent absorption peaks (Figure 5). Specifically, the peaks at 3235.32 cm^{-1} and 1066.00 cm^{-1} correspond to vibrational modes of hydroxyl groups in carboxylic acid and primary alcohol functionalities, respectively. These values differed from the corresponding peaks at 3287.50 cm^{-1} and 1080.90 cm^{-1} observed in the original orange peel extract FTIR analysis, indicating changes in the functional groups during nanoparticle synthesis.

Furthermore, the FTIR spectrum (Figure 5) exhibited distinct vibrational modes, including aromatic ring deformations at 1602.73 cm^{-1}, which were red shifted from 1636.30 cm^{-1}, and vinyl bending vibrations at 969.10 cm^{-1}, shifted from 998.90 cm^{-1}. A prominent alkyne stretch was observed at 2109.67 cm^{-1}, alongside aliphatic C-H stretches at 1077.85 cm^{-1} and sulfonate group vibrations at 1371.66 cm^{-1}. These spectral features indicate significant molecular modifications, revealing a complex molecular structure.

The reduction of ferric/ferrous chloride solution, marked by noticeable color changes during synthesis, can be attributed to the presence of hydroxyl and alkene functional groups (Gulcin, 2015). Furthermore, the appearance of a distinct peak at 693.30 cm^{-1}, indicative of iron-oxygen bond vibrations, provided conclusive evidence for the successful synthesis of iron oxide nanoparticles, consistent with the metal-oxygen bond spectrum range of 400-850 cm^{-1} (Karpagavinayagam and Vedhi, 2019). This finding is also supported by the similar band noted at 677 cm^{-1} for Fe-O stretching vibration (Liang *et al*., 2020).

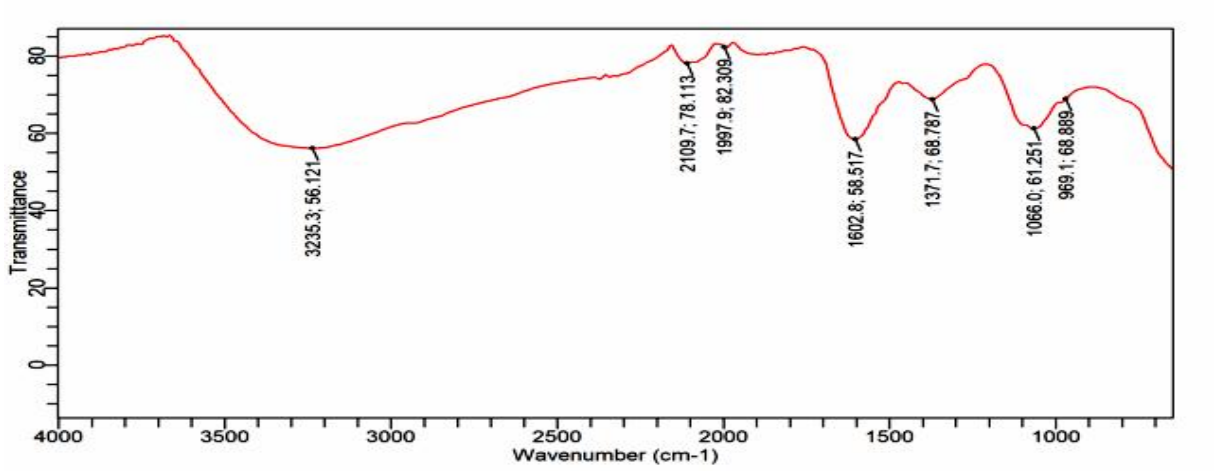

Figure 5: FTIR spectrum of the iron oxide nanoparticles

The scanning electron microscopy (SEM) examination of the nanoparticles at magnifications of 8000, 9000, and 10000 (refer to Plate I) unveiled a non-uniform, irregular shape with visible signs of iron oxide nanoparticles (Fe_3O_4) aggregation. At 8000x magnification, the particles displayed a smooth surface that evolved into rough and non-uniform surfaces, indicating aggregation. This observation is in line with the Polydispersity Index (PDI) of 0.547 from the dynamic light scattering (DLS) analysis, suggesting aggregation likely triggered by

DOI: 10.56892/bima.v8i4.1151

dipole-dipole interactions among the particles (Da'na *et al*., 2018).

Comparable results were obtained by Sudhakar *et al*. (2022) for nanoparticles synthesized using *Simarouba Glauca* leaf extract. Analysis using ImageJ software revealed a particle size distribution ranging from 7.05 to 44.18 nm, with a mean particle size of 22.92 nm. Although this value is slightly lower than the DLS-derived measurements, it falls within the expected size range for these nanoparticles.

Energy Dispersive X-ray Spectroscopy (EDS) analysis of the orange peel nanoparticles detected distinct emission energies at 2 KeV, which corresponds to the binding energy of iron (Fe) (Plate II). The EDS spectrum revealed that iron comprised 78.65% of the nanoparticle composition. Additionally, oxygen was detected at 0.1 KeV with a percentage of 20.02%, and a minor peak was observed at 0.5 KeV for carbon at 2.22%.

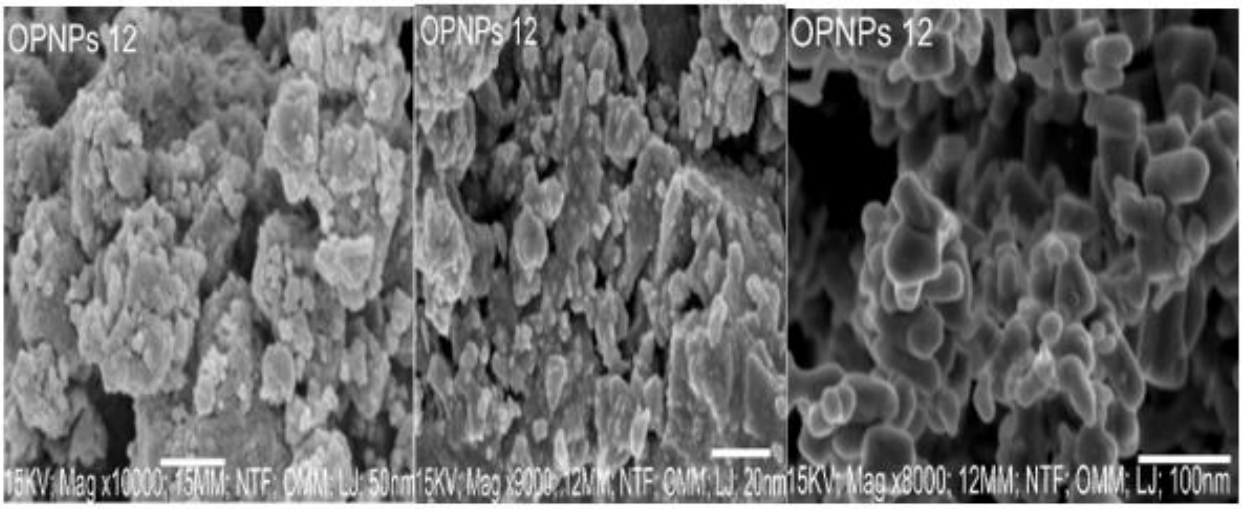

Plate I: SEM image of the iron oxide nanoparticles

Bima Journal of Science and Technology, Vol. 8(4A) Dec, 2024 ISSN: 2536-6041

DOI: 10.56892/bima.v8i4.1151

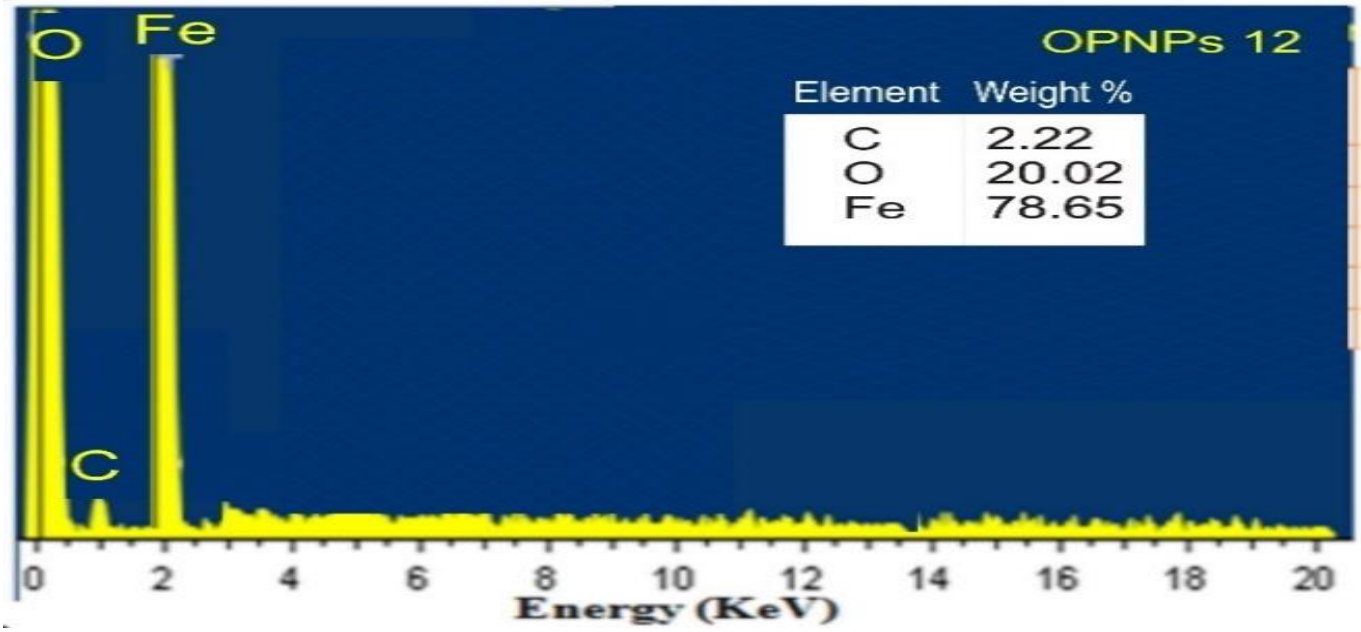

Plate II: EDS result of the iron oxide nanoparticles.

X-Ray Diffraction (XRD) analysis was employed to investigate the crystallographic properties of iron oxide nanoparticles derived from orange peel extract. The XRD spectrum, analyzed using X'Pert HighScore, is presented in Figure 6. The spectrum exhibits distinct diffraction maxima at 2θ angles of 30.48, 35.78, 43.34, 53.60, and 63.22 degrees. The dominant peak at 35.78 degrees, with a maximum intensity of 100%, indicates the formation of highly crystalline magnetite (Fe_3O_4), consistent with previous study reported by Aliout *et al*., (2023). The diffraction maxima were indexed to specific crystal planes, denoted by Miller indices of (022), (113), (004), (224), and (044), respectively. The XRD profile matches the ICSD collection code 77592 and reference code 98-006-1958, as well as the PDF data for Fe_3O_4 (ICSD 01-071-6339), confirming a cubic crystal structure with an FD-3M space group. The crystal size, calculated using the Debye-Scherrer equation, was determined to be 45.91 nm, indicating that the synthesized particles are within the nanoscale range. This result is consistent with the DLS analysis Z-average of 42.60 nm, although it differs from the SEM-derived size of 22.92 nm (range: 7.05-44.18 nm). The successful production of iron oxide nanoparticles at the nanoscale was confirmed by all analyses. The XRD results are in agreement with previous studies that employed coprecipitation methods for synthesizing iron oxide nanoparticles (Paul *et al*., 2022; Arief *et al*., 2023; Gogoi, 2023).

DOI: 10.56892/bima.v8i4.1151

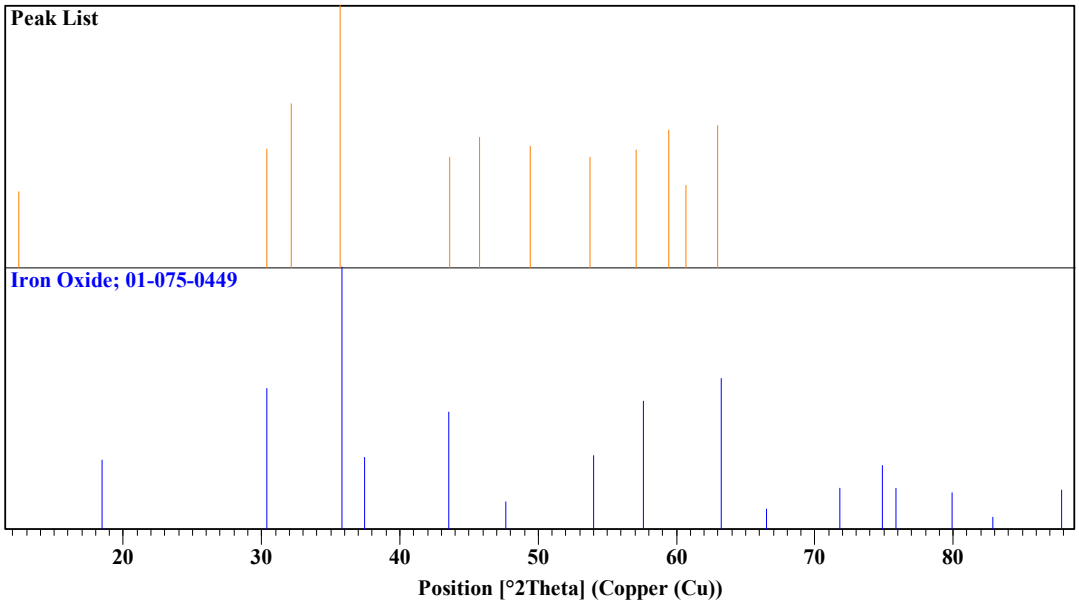

Figure 6: XRD diffractogram of the iron oxide nanoparticles

The BET analysis of the IONPs synthesized from orange peel extract revealed a remarkably large surface area of 925.2 m^2/g, accompanied by a Langmuir surface area of 60.52 m^2/g. This suggests that the nanoparticles possess a porous structure with irregular shapes and size distributions, consistent with DLS analysis findings (Figures 3 and 4). The exceptionally large surface area may be attributed to the presence of organic compounds in the orange peel extract, which likely acted as capping agents or stabilizers during synthesis, resulting in rough and irregular nanoparticle surfaces (Hani *et al*., 2024). The enhanced surface roughness contributes significantly to the overall surface area, potentially amplified by nanoparticle porosity introduced during extraction or synthesis (Khdary *et al*., 2023). The internal pores within the nanoparticles provide additional sites for gas adsorption, contributing to the high BET surface area. The coprecipitation method employed facilitates rapid nucleation and growth of iron oxide nanoparticles under alkaline conditions, yielding high crystallinity and surface area (Trifoi *et al*., 2023)

Batch Adsorption experiments

Effect of adsorbent dose and contact time

As shown in Fig. 7, the optimal adsorption conditions were achieved with an adsorbent dose of 100 mg and a shaking time of 15 min, resulting in the removal of 97.69% of ibuprofen by the iron oxide nanoparticles synthesized from orange peel extract. It was observed that increasing the adsorbent dose from 20-100 mg led to a corresponding increase in the amount adsorbed. However, further increases in adsorbent dose beyond the optimal level did not result in additional adsorption, indicating a saturation point had been reached.

Increasing the adsorbent dose means increasing the available surface area and active sites for the adsorption of the adsorbate which resulted in enhancement of nanoparticle's removal efficiency and adsorption capacity. However, beyond a certain point, the adsorbent dose may not have a significant

DOI: 10.56892/bima.v8i4.1151

effect on ibuprofen removal due to saturation of adsorption sites, adsorbent particles overlapping and pores blockage (Rafati *et al*., 2018). This was observed after the optimum adsorption was attained which shows no further increase in adsorption of ibuprofen. Increase in the contact time allows more time for the ibuprofen molecules to diffuse from the bulk solution onto adsorbent surface and into the pores. Upon reaching equilibrium, the adsorption capacity remains unaffected by contact time, indicating no net transfer of the adsorbate between the solution and the adsorbent (Ngernyen *et al*., 2023).

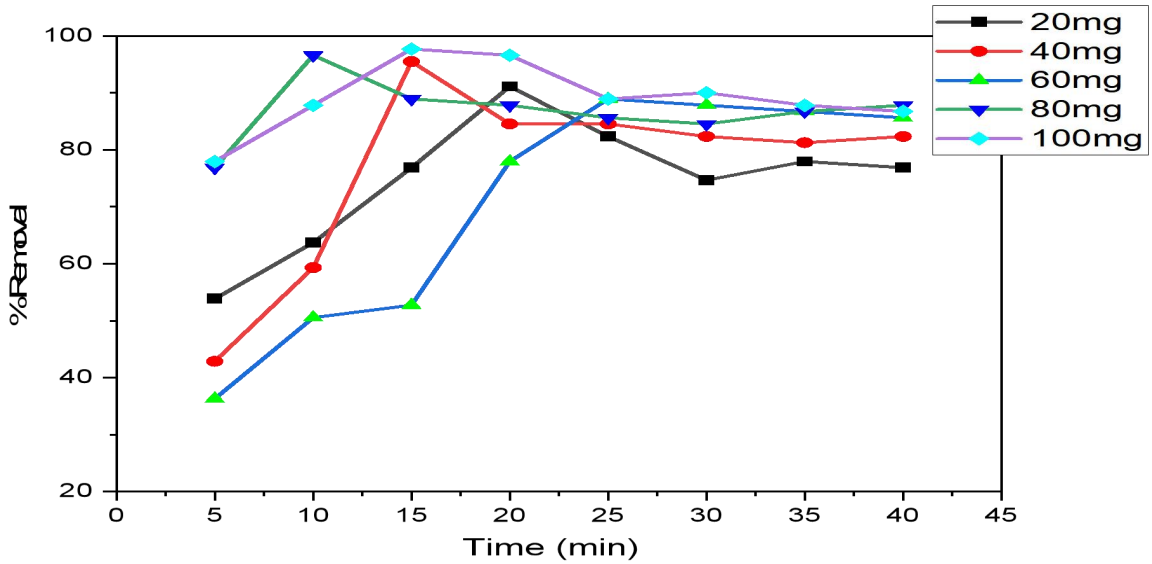

Figure 7: Result of the effect of contact time and adsorbent dose on the removal of ibuprofen with the IONPs

Effect of initial concentration

As presented in Fig.8 above, the optimum adsorbate concentration was 2 ppm achieving removal efficiency of 89.80% of the adsorbate using the iron oxide nanoparticles. However, amount of ibuprofen adsorbed did not follow a definite pattern with increased in initial concentration, hence, the increase in initial concentration of ibuprofen has a negligible influence on ibuprofen removal using the adsorbent. This agrees with the findings of Nguyen *et al*., (2019) for metal- organic framework, initial concentration of 10 mg/L was utilized and it was observed that the initial concentration of ibuprofen solution shows a negligible effect on the ibuprofen removal efficiency.

DOI: 10.56892/bima.v8i4.1151

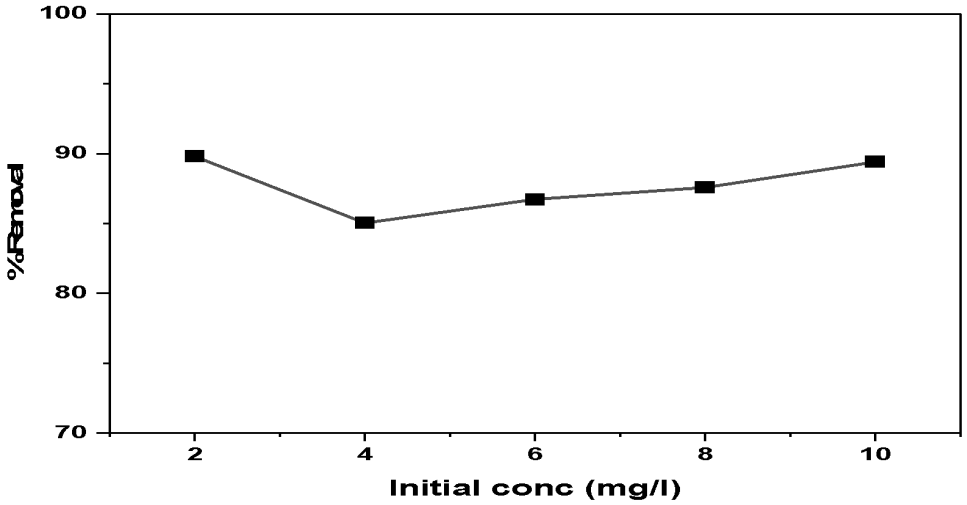

Figure 8: Effect of initial concentration of ibuprofen on it removal from water using the IONPs

The effect of pH on the adsorption of ibuprofen using the synthesized iron oxide nanoparticles

The pHpzc (point of zero charge) of iron oxide nanoparticles (IONPs) affects ibuprofen adsorption from water. Below pHpzc, IONPs' positive surface charge attracts negatively charged ibuprofen, enhancing adsorption. Above pHpzc, the negative surface charge repels ibuprofen, reducing adsorption (Nguyen *et al*., 2019; Bhadra *et al*., 2017). Ibuprofen's ionization state, influenced by pH and its pKa (5.2), also impacts adsorption. Neutral ibuprofen (below pKa) sorbs more easily onto IONPs, while anionic ibuprofen (above pKa) remains in solution (Ulfa *et al*., 2021).

The adsorption behavior of ibuprofen on iron oxide nanoparticles (IONPs) is significantly influenced by pH-mediated electrochemical interactions. The pH-dependent surface charge of IONPs affects its attraction to ibuprofen molecules, while pH also alters the ionization state and speciation of ibuprofen, impacting its binding characteristics (Garau *et al*., 2019). The point of zero charge (pHpzc) of IONPs, occurring at pH 6.9, plays a crucial role in adsorption processes. Below pHpzc, the positively charged IONPs attract negatively charged ibuprofen, enhancing adsorption. Above pHpzc, the negatively charged surface repels ibuprofen, reducing adsorption (Nguyen *et al*., 2019; Bhadra *et al*., 2017).

Ibuprofen's ionization state, influenced by pH and its pKa (5.2), also impacts adsorption. Neutral ibuprofen (below pKa) sorbs more easily onto IONPs, while anionic ibuprofen (above pKa) remains in solution (Ulfa *et al*., 2021). Optimal ibuprofen adsorption on orange peel-derived IONPs (OPNPs) occurred at pH 7, with a maximum adsorption capacity of 79% (Fig. 10). This finding is consistent with previous studies, which suggest that optimal ibuprofen adsorption typically occurs at pH levels corresponding to the adsorbent's point of zero charge (PZC) (Sandoval-González *et al*., 2022; Osman *et al*., 2024).

Bima Journal of Science and Technology, Vol. 8(4A) Dec, 2024 ISSN: 2536-6041

DOI: 10.56892/bima.v8i4.1151

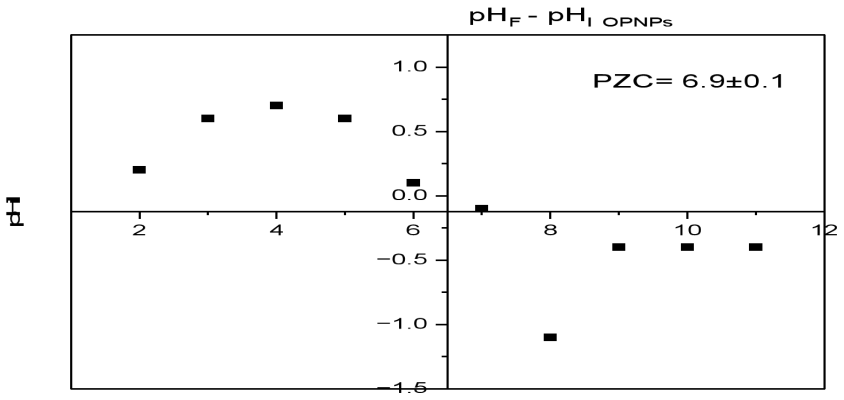

Figure 9: pH_{pzc} analysis of the iron oxide nanoparticles

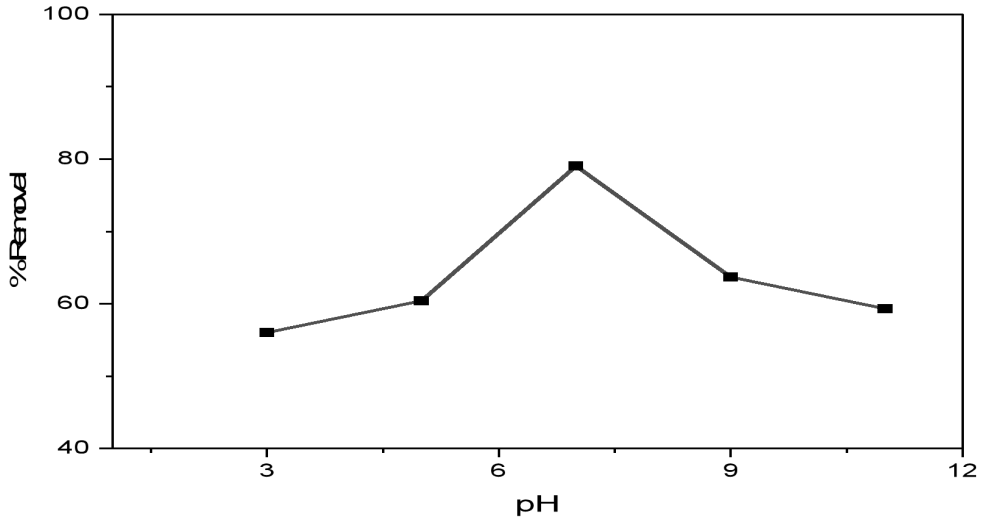

Figure 10: Effect of pH on the removal of ibuprofen.

Effect of Temperature on the adsorption of Ibuprofen

Figure 11 demonstrates a consistent trend of decreasing ibuprofen adsorption as temperature increases for the iron oxide nanoparticle types (80.15-59.32%). This observation suggests that higher temperatures may have an adverse impact on the adsorption efficiency of these nanoparticles (Rata *et al*., 2023). Despite the overall decline, minor fluctuations in the percentage of ibuprofen adsorbed at specific temperatures are evident for the iron oxide nanoparticle. These variations may stem from differences in the physical and chemical attributes of the nanoparticles, such as surface area, porosity, and functional groups, which interact with ibuprofen molecules (Boruah *et al*., 2023).

The reduction in removal with rise in temperature could be linked to the heightened kinetic energy of ibuprofen molecules, potentially resulting in reduced interaction

DOI: 10.56892/bima.v8i4.1151

time with the nanoparticle surfaces or desorption of ibuprofen from said surfaces. As the temperature increases, the interactions between ibuprofen molecules and the adsorbent can weaken, leading to a reduction in adsorption capacity (Sadegh *et al*., 2017).

The solubility of ibuprofen in water may rise with temperature, leading to a greater ibuprofen concentration in the solution and a diminished tendency to adsorb onto solid phases. The adsorbent's physical and chemical properties could also undergo alterations with temperature, potentially reducing the presence of active sites for adsorption (Osman *et al*., 2024). At elevated temperatures, other substances in the solution may become more competitive for adsorption sites, displacing ibuprofen molecules.

These factors suggest that the adsorption of ibuprofen onto nanoparticles is likely exothermic, where the process releases heat, indicating that higher temperatures do not favor adsorption (Osman *et al*., 2024). This stands in contrast to endothermic processes like ciprofloxacin adsorption, which benefit from higher temperatures.

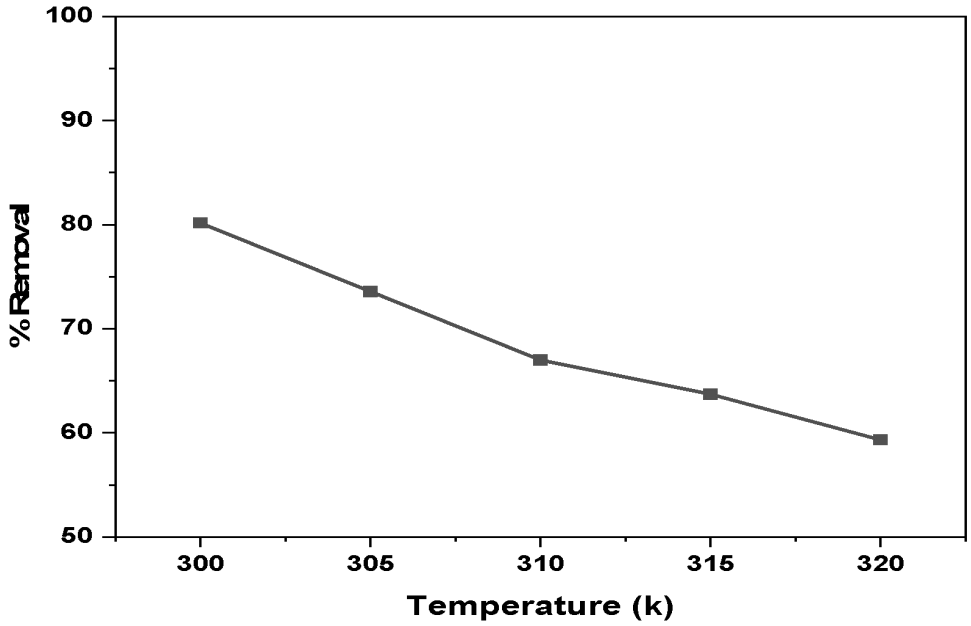

Figure 11: Effect of temperature on the adsorption of Ibuprofen

Determination and remediation of ibuprofen in domestic wastewater using the iron oxide nanoparticles

As presented on Fig 12, the concentration of ibuprofen of 0.68, 1.30, and 1.14 mg/L respectively for the sample locations. The adsorption showed a significant reduction in the concentration of ibuprofen across all samples after treatment with iron oxide nanoparticles. For Sample A, the concentration decreased from 0.68 mg/L to 0.0544 mg/L, which translates to a reduction of approximately 92%. Similarly, Sample B saw a decrease from 1.30 mg/L to 0.1101 mg/L, a reduction of about 91.5%. Sample C experienced a reduction from 1.14 mg/L to 0.1200 mg/L, which is around 89.5%. These results highlight the effectiveness of iron oxide nanoparticles in removing ibuprofen from

DOI: 10.56892/bima.v8i4.1151

wastewater, achieving an average reduction of about 91%.

The high percentage reductions observed in all samples underscore the potential of iron oxide nanoparticles as a treatment method for pharmaceutical contaminants in wastewater. The nanoparticles likely facilitate the adsorption and degradation of ibuprofen, thereby significantly lowering its concentration. This effectiveness is crucial for developing sustainable and efficient wastewater treatment technologies, especially in regions where pharmaceutical contamination is a growing concern (Parveen *et al*., 2021).

One of the notable aspects of the results is the consistency in the reduction of ibuprofen concentration across different samples. All samples showed reductions above 89%, indicating that the treatment method is reliable and can be expected to perform consistently in various conditions. This consistency is essential for practical applications, as it ensures that the treatment method can be scaled up and applied in real-world scenarios with predictable outcomes.

Generally, the results of the study indicate that the concentrations of ibuprofen in domestic wastewater vary according to the population density of the area. The highest concentrations of the ibuprofen was found in the middle density populated area (B), followed by the high-density populated area (C), and the lowest concentrations were found in the low-density populated area (A). This suggests that the consumption of these drugs is higher in more populated areas, and that the wastewater treatment processes are not efficient enough to remove them completely.

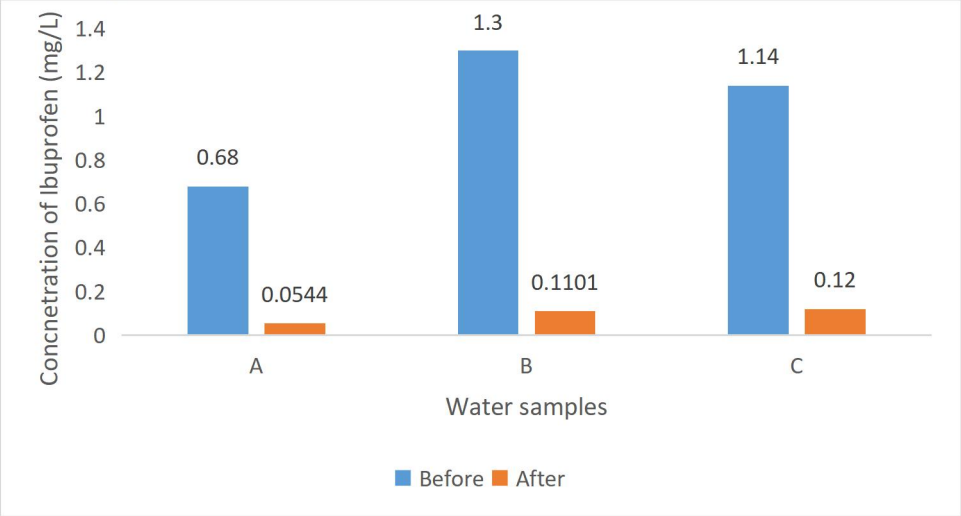

Figure 12: Concentration of ibuprofen in domestic wastewater before and after treatment

Thermodynamic studies for the adsorption of ibuprofen

Gibbs free energy (ΔG) measures the spontaneity of the adsorption process. Negative ΔG values (Table 1) indicate that the process is spontaneous. The significantly negative ΔG values for OPNPs (-53701.71 J/mol, -4890.96 J/mol, -4411.22 J/mol, -3931.47 J/mol, -3451.72 J/mol) suggest a highly spontaneous adsorption of ibuprofen onto iron oxide nanoparticles, indicating a strong affinity between the ibuprofen molecules and the IONPs (Osman *et al*., 2024; Campos *et al*., 2020).

Enthalpy (ΔH) reveals the heat change during adsorption. The negative ΔH value (-34155.78 J/mol) shows that the process is exothermic, meaning heat is released during ibuprofen

DOI: 10.56892/bima.v8i4.1151

adsorption onto the IONPs (Osman *et al*., 2024). Exothermic adsorption is typically linked to physical adsorption, involving van der Waals forces or hydrogen bonding (Campos *et al*., 2020).

Entropy (ΔS) indicates the level of disorder at the solid-liquid interface during adsorption. The negative ΔS value (-95.95 J/mol) suggests a decrease in randomness at the interface during ibuprofen adsorption onto the OPNPs (Sellaoui *et al*., 2016). This decrease in entropy may result from the orderly arrangement of ibuprofen molecules on the nanoparticle surface, indicating a structured adsorption process (Quaino *et al*., 2022; Osman *et al*., 2024).

Table 1: The thermodynamic parameters for the adsorption of ibuprofen

Adsorbent	ΔG (J/mol)	ΔH (J/mol)	ΔS (J/mol)
OPNPs	-53701.71		
	-4890.96		
	-4411.22	-34155.78265	-95.9502112
	-3931.47		
	-3451.72		

Adsorption of isotherms of ibuprofen using the synthesized IONPs

The Langmuir isotherm model characterizes adsorption as a uniform monolayer formation on a surface with a limited number of equivalent sites (Chen, 2015). Table 2 presents the Langmuir isotherm parameters for iron oxide nanoparticles (IONPs), including: a maximum adsorption capacity (q_m) of 11.5314 mg/g, representing the highest amount of ibuprofen that can be adsorbed per unit mass of adsorbent; a Langmuir affinity constant (K_L) of 0.5164 L/mg, indicating a strong binding affinity between the adsorbate and adsorbent; a favorability factor (R_L) of 0.01941, with values within the 0-1 range signifying favorable adsorption conditions; and a coefficient of determination (R^2) of 0.93461, confirming an excellent agreement between experimental data and the Langmuir isotherm model (Chen, 2015).

In contrast, the Freundlich isotherm model describes adsorption on a heterogeneous surface with sites of varying affinities (Vigdorowitsch *et al*., 2021). As shown in Table 2, the Freundlich isotherm parameters include: the heterogeneity factor (1/n) at 0.90895, indicating a relatively heterogeneous surface; the adsorption intensity (n) at 1.10017, representing the strength of adsorption; and the Freundlich constant (K_F) at 4.32245 (mg/g) $(l/mg)^{1/n}$), characterizing the adsorption capacity. The fit of the experimental data to the Freundlich isotherm model is characterized by a coefficient of determination (R^2) of 0.90328, revealing a moderate level of consistency between the observed and predicted value, although slightly lower than the Langmuir model (Campos *et al*., 2020).

The Temkin isotherm model posits that the adsorption energy diminishes in a linear fashion as surface coverage increases, resulting from interactions between the adsorbent and adsorbate. Table 2 lists the Temkin isotherm parameters, including the adsorption energy term (RT/b), which has a value of 0.90895, representing the change in heat of adsorption as a function of surface coverage; (ln (a)), the Temkin constant, at 1.46382; (a), the equilibrium binding constant, at 4.32244 L/g; and (b), the Temkin constant related to the heat of adsorption, at 2727.12 J/mol. A coefficient of determination (R^2) of 0.90328 is obtained for the Temkin isotherm model, indicating a moderate level of consistency between the experimental data and the model's predictions, supporting the assumption of a linear decrease in heat of

DOI: 10.56892/bima.v8i4.1151

adsorption with surface coverage, resulting from adsorbent-adsorbate interactions

The adsorption of ibuprofen onto IONPs is effectively described by the Langmuir, Freundlich, and Temkin isotherm models, all showing high correlation coefficients. The Langmuir model suggests monolayer adsorption with a high maximum capacity and favorable conditions (Osman *et al*., 2024). The Freundlich model suggests adsorption on a heterogeneous surface, whereas the Temkin model reveals a decrease in the heat of adsorption with increasing coverage. These findings demonstrate the efficacy of OPNPs as an adsorbent for ibuprofen, providing valuable insights into the underlying adsorption mechanisms and their potential applications in wastewater treatment (Campos *et al*., 2020).

Table 2: The adsorption isotherms parameters for the adsorption of ibuprofen

S/N	Isotherm	Parameters	Values
1	Langmuir	q_m(mg/g)	11.5314
		K_L(L/mg)	0.5164
		R_L (mg/l)	0.01941
		R^2	0.93461
2	Freundlich	1/n	0.90895
		n	1.10017
		K_F(mg/g)(l/mg)$^{1/n}$	4.32245
		R^2	0.90328
3	Temkin	RT/b	0.90895
		ln(a)	1.46382
		a(L/g)	4.32244
		b(J/mol)	2727.12
		R^2	0.90328

Kinetic equilibrium studies of Ibuprofen using the synthesized IONPs

The pseudo-first-order kinetic model describes an adsorption process in which the rate of surface coverage is linearly dependent on the availability of unoccupied sites. As shown in Table 3, the model's parameters are: an equilibrium adsorption capacity (qe) of 3.68190 mg/g, a rate constant (k_1) of -0.00157 min^{-1}, and a correlation coefficient (R^2) of 0.72670. However, the relatively low R^2 value and negative k_1 value suggest that the experimental data deviate from the pseudo-first-order model, indicating a poor fit and potential limitations of this kinetic framework in describing the adsorption process (Sha'aran *et al*., 2019).

The pseudo-second-order kinetic model emphasizes the crucial interplay between adsorption site availability and adsorbate-adsorbent interactions. The model's key parameters include: an equilibrium adsorption capacity (q_e) of 5.94919 mg/g, a secondary equilibrium value (q_e^2) of 35.39290 mg/g, a rate constant (k_2) of 0.01318 g/mg.min, and a high correlation coefficient (R^2) of 0.92174. These parameters demonstrate an excellent fit with the experimental data, indicating that this model provides a more accurate representation of the adsorption process, capturing the complex dynamics between adsorbate and adsorbent (Kostoglou *et al*., 2022).

The interparticle diffusion model examines the transport of adsorbate molecules within the adsorbent's pores. The model's key parameters,

DOI: 10.56892/bima.v8i4.1151

as shown in Table 2, include the intraparticle diffusion rate constant (k_p) with units of mg/g.min$^{1/2}$, the intercept (C) in mg/g, and a correlation coefficient (R^2) of 0.84304. These results indicate that intraparticle diffusion plays a significant role in the adsorption process, although the moderate R^2 value suggests that other factors may also influence the adsorption kinetics, and intraparticle diffusion may not be the sole rate-controlling mechanism (Musah *et al*., 2022).

The Elovich model, frequently employed to examine chemisorption phenomena on diverse surfaces (López-Luna *et al*., 2019), provides insights through parameters such as the initial adsorption rate (α) of 0.92973 mg/g.min, the desorption coefficient (β) of 0.71237 g/mg, and a coefficient of determination (R^2) of 0.87050. The notable congruence between the Elovich model and experimental findings suggests that chemisorption plays a pivotal role in the adsorption process, highlighting the crucial impact of surface saturation and energy barriers on the adsorption kinetics.

The kinetic parameters indicate that the pseudo-second-order kinetic model best describes the adsorption of ibuprofen onto IOPNPs, as evidenced by the high correlation coefficient (R^2 = 0.92174) (Table 3). This suggests that the adsorption process is primarily influenced by the availability of adsorption sites and the interactions between ibuprofen molecules and IOPNPs (Oputu *et al*., 2022). Additionally, the interparticle diffusion and Elovich models provide valuable insights, revealing that intraparticle diffusion and chemisorption play significant roles in the adsorption process. In contrast, the pseudo-first-order model shows poor alignment with the experimental data, implying that it is unlikely to be the primary mechanism governing ibuprofen adsorption onto IOPNPs (Ali *et al*., 2023).

Table 3: Kinetic models for the adsorption of ibuprofen using the synthesized IONPs

S/N	Isotherm	Parameters	OPNPs
1	Pseudo 1st order	q_e(mg/g)	3.68190
		k_1(min^{-1})	-0.00157
		R^2	0.72670
2	Pseudo 2nd order	q_e(mg/g)	5.94919
		q_e^2	35.39290
		k_2(g/mgmin)	0.01318
		R^2	0.92174
3	Interparticle diffusion	k_p(mg/gmin$^{1/n}$)	0.69332
		C (mg/g)	0.38175
		R^2	0.84304
4	Elovich	α(mg//gmin)	0.92973
		β (g/mg)	0.71237
		R^2	0.87050

CONCLUSION

The results highlighted the significant impact of factors such as adsorbent dose, initial ibuprofen concentration, contact time, pH, and temperature on the adsorption process. IONPs achieved an impressive average removal efficiency of over 89% for ibuprofen, with adsorption kinetics conforming to a pseudo-

DOI: 10.56892/bima.v8i4.1151

second-order model and isotherm analysis revealing monolayer coverage consistent with the Langmuir model. The optimum adsorption were achieved at initial ibuprofen concentration of 10 mg/L, contact time of 15 min, pH of 7, adsorbent dose of 100 mg at room temperature. Thermodynamic evaluations confirmed spontaneous and exothermic adsorption, suggesting optimal removal at lower temperatures. The concentration of ibuprofen in wastewater samples (A, B, and C) was also significantly reduced after treatment with iron oxide nanoparticles. Initial concentrations (0.68, 1.30, and 1.14 mg/L) decreased to 0.0544, 0.1101, and 0.1200 mg/L, respectively, achieving reductions of 92%, 91.5%, and 89.5%. On average, iron oxide nanoparticles removed approximately 91% of ibuprofen from the wastewater samples. Hence, this research contributes meaningfully to wastewater treatment knowledge, emphasizing IONPs' reliable performance and scalability for practical applications. Future studies could investigate their long-term stability, regeneration potential, and effectiveness against other pharmaceutical pollutants to further enhance this eco-friendly treatment approach.

Acknowledgement

The authors acknowledge the financial support provided by the Tertiary Education Trust Fund (TETFund) through the Institutional Based Research (IBR) grant at Kaduna State University.

REFERENCES

Abdullaeva, Z. (2017). Purification on Nanomaterials. In: Synthesis of Nanoparticles and Nanomaterials. Springer, Cham. https://doi.org/10.1007/978-3-319-54075-7_7

Abdullah, J. A. A., Jiménez-Rosado, M., Perez-Puyana, V., Guerrero, A., & Romero, A. (2022). Green synthesis of FexOy nanoparticles with potential antioxidant properties. *Nanomaterials*, *12*(14), 2449.

Afonso, R., Gales, L., & Mendes, A. (2016). Kinetic derivation of common isotherm equations for surface and micropore adsorption. *Adsorption*, *22*, 963-971. https://doi.org/10.1007/s10450-016-9803-z

Ahmadpour, A., Fallah, S., and Towfighi, J. (2019). Synthesis and characterization of nanostructured NiO/Al_2O_3 catalyst for oxidative dehydrogenation of ethane. Journal of the Iranian Chemical Society, 16(2), 299-310. https://doi.org/10.1007/s13738-018-1510-4.

Aliouat, E., Belmokhi, N., Mihoubi, B., Filali, H., Bouhroum, R., & Boukheit, N. (2023, October). Synthesis and Characterization of Nickel Doped Fe_3O_4 Nanoparticles Using Solvothermal Method. In *International Conference of Nanotechnology for Environmental Protection and Clean Energy Production* (pp. 185-195). Singapore: Springer Nature Singapore. https://doi.org/10.1007/978-981-97-1916-7_19

Arief, S., Muldarisnur, M., and Usna, S. R. (2023). Enhancement in photoluminescence performance of carbon-based Fe_3O_4@ ZnO–C nanocomposites. *Vacuum*, 211, 111935.

Bakatula, E.N., Richard, D., Neculita, C.M. and Zagury, G.J. (2018). Determination of point of zero charge of natural organic materials. *Environmental Science and Pollution Research*, *25*, 7823-7833.

DOI: 10.56892/bima.v8i4.1151

https://doi.org/10.1007/s11356-017-1115-7\

Baptista, A. C., Brito, M., Marques, A., & Ferreira, I. (2021). Electronic control of drug release from gauze or cellulose acetate fibres for dermal applications. *Journal of Materials Chemistry B*, *9*(16), 3515-3522. https://doi.org/10.1039/D1TB00249J

Batucan, N. S. P., Tremblay, L. A., Northcott, G. L., & Matthaei, C. D. (2022). Medicating the environment? A critical review on the risks of carbamazepine, diclofenac and ibuprofen to aquatic organisms. *Environmental Advances*, *7*, 100164. https://doi.org/10.1016/j.envadv.2021.100164

Bhadra, B. N., Ahmed, I., Kim, S., and Jhung, S. H. (2017). Adsorptive removal of ibuprofen and diclofenac from water using metal-organic framework-derived porous carbon. *Chemical Engineering Journal*, 314, 50-58. https://doi.org/10.1016/j.cej.2016.12.127

Boruah, H., Tyagi, N., Gupta, S. K., Chabukdhara, M., & Malik, T. (2023). Understanding the adsorption of iron oxide nanomaterials in magnetite and bimetallic form for the removal of arsenic from water. *Frontiers in Environmental Science*, *11*, 1104320. https://doi.org/10.3389/fenvs.2023.1104320

Brillas, E. (2022). A critical review on ibuprofen removal from synthetic waters, natural waters, and real wastewaters by advanced oxidation processes. *Chemosphere*, *286*, 131849. https://doi.org/10.1016/j.chemosphere.2021.131849

Chen, X. (2015). Modeling of experimental adsorption isotherm data. *Information*, *6*(1), 14-22. https://doi.org/10.3390/info6010014

Da'na, E., Taha, A., and Afkar, E. (2018). Green synthesis of iron nanoparticles by Acacia nilotica pods extract and its catalytic, adsorption, and antibacterial activities. *Applied Sciences*, 8(10), 1922

Dadfar, S. M., Camozzi, D., Darguzyte, M., Roemhild, K., Varvarà, P., Metselaar, J., ... & Lammers, T. (2020). Size-isolation of superparamagnetic iron oxide nanoparticles improves MRI, MPI and hyperthermia performance. *Journal of nanobiotechnology*, *18*, 1-13.

Dalal, N., Boruah, B. S., Neoh, A., & Biswas, R. (2019). Correlation of surface plasmon resonance wavelength (SPR) with size and concentration of noble metal nanoparticles. *Annals of Reviews and Research*, *5*(2), 50-55.

Faisal, S., Jan, H., Shah, S. A., Shah, S., Khan, A., Akbar, M. T., Rizwan, M., Jan, F., Wajidullah, and Akhtar, N. (2021). Green synthesis of zinc oxide (ZnO) nanoparticles using aqueous fruit extracts of Myristica fragrans: their characterizations and biological and environmental applications. *ACS Omega*, 6(14), 9709–9722. https://doi.org/10.1021/acsomega.1c00310

Garau, G., Lauro, G. P., Diquattro, S., Garau, M., and Castaldi, P. (2019). Sb (V) adsorption and desorption onto ferrihydrite: influence of pH and competing organic and inorganic anions. *Environmental Science and Pollution Research*, *26*, 27268-27280. https://doi.org/10.1007/s11356-019-05919-z

Gogoi, B. (2023). Synthesis and Characterisation of Transition Metal Iron Oxide Nanocomposite Crystals

DOI: 10.56892/bima.v8i4.1151

and Particles Using Wet Chemical Coprecipitation Method. *Protection of Metals and Physical Chemistry of Surfaces*, *59*(6), 1200-1209. https://doi.org/10.1134/S2070205123701149

Govindarajan, D. K., Selvaraj, V., Selvaraj, A. S. J. M., Hameed, S. S., Pandiarajan, J., & Veluswamy, A. (2023). Green synthesis of silver micro-and nano-particles using phytochemical extracts of Cymbopogon citratus exhibits antibacterial properties. *Materials Today: Proceedings*, *76*, 103-108. https://doi.org/10.1016/j.matpr.2022.10.133

Gülçin, İ. (2015). Fe 3+–Fe 2+ transformation method: an important antioxidant assay. *Advanced protocols in oxidative stress III*, 233-246. https://doi.org/10.1007/978-1-4939-1441-8_17

Guo, Y., Sun, Q., Wu, F. G., Dai, Y., & Chen, X. (2021). Polyphenol-containing nanoparticles: synthesis, properties, and therapeutic delivery. *Advanced Materials*, *33*(22), 2007356.

Hani, U., Kidwan, F. N., Albarqi, L. A., Al-Qahtani, S. A., AlHadi, R. M., AlZaid, H. A., ... & Ansari, M. A. (2024). Biogenic silver nanoparticle synthesis using orange peel extract and its multifaceted biomedical application. *Bioprocess and Biosystems Engineering*, 1-13. https://doi.org/10.1007/s00449-024-03031-2

Ishak, N. M., Kamarudin, S. K., and Timmiati, S. N. (2019). Green synthesis of metal and metal oxide nanoparticles via plant extracts: an overview. *Materials Research Express*, 6(11), 112004. DOI 10.1088/2053-1591/ab4458

Jadoun, S., Arif, R., Jangid, N. K., & Meena, R. K. (2021). Green synthesis of nanoparticles using plant extracts: A review. *Environmental Chemistry Letters*, *19*(1), 355-374. https://doi.org/10.1007/s10311-020-01074-x

Jan-Roblero, J., & Cruz-Maya, J. A. (2023). Ibuprofen: toxicology and biodegradation of an emerging contaminant. *Molecules*, *28*(5), 2097. https://doi.org/10.3390/su15021613

Jeevanandam, J., Kiew, S. F., Boakye-Ansah, S., Lau, S. Y., Barhoum, A., Danquah, M. K., and Rodrigues, J. (2022). Green approaches for the synthesis of metal and metal oxide nanoparticles using microbial and plant extracts. *Nanoscale*, 14(7), 2534-2571.

Kajjumba, G. W., Emik, S., Öngen, A., Özcan, H. K., & Aydın, S. (2018). Modelling of adsorption kinetic processes—errors, theory and application. *Advanced sorption process applications*, 1-19.

Karpagavinayagam, P., and Vedhi, C. (2019). Green synthesis of iron oxide nanoparticles using Avicennia marina flower extract. *Vacuum*, 160, 286-292. https://doi.org/10.1016/j.vacuum.2018.11.043

Katare, A. K., Tabassum, A., Sharma, A. K., & Sharma, S. (2023). Treatment of pharmaceutical wastewater through activated sludge process—a critical review. *Environmental Monitoring and Assessment*, *195*(12), 1466. https://doi.org/10.1007/s10661-023-11967-3

Khdary, N. H., Almuarqab, B. T., & El Enany, G. (2023). Nanoparticle-embedded polymers and their applications: a review. *Membranes*, *13*(5), 537. https://doi.org/10.3390/membranes13050537

Kostoglou, M., & Karapantsios, T. D. (2022). Why is the linearized form of pseudo-second order adsorption kinetic model

DOI: 10.56892/bima.v8i4.1151

so successful in fitting batch adsorption experimental data?. *Colloids and Interfaces*, *6*(4), 55. https://doi.org/10.3390/colloids6040055

Kumari, A., Yadav, A., Singh, O. P., & Sharan, P. (2024). A Review Of Surface Plasmon Resonance (SPR) Technology In Biosensing: Innovations, Applications And Future Trends. *Journal of Optics*, 1-9.

Kupina, S., Fields, C., Roman, M. C., and Brunelle, S. L. (2018). Determination of total phenolic content using the Folin-C assay: single-laboratory validation, first action 2017.13. *Journal of AOAC International*, 101(5), 1466-1472. https://doi.org/10.5740/jaoacint.18-0031

Liang, Y., Jiang, L., Xu, S., Ju, W., Tao, Z., Yang, Y., ... & Wei, G. (2024). Synthesis and characterization of Fe3O4 nanoparticles prepared by solvothermal method. *Journal of Materials Engineering and Performance*, *33*(13), 6804-6815. https://doi.org/10.1007/s11665-023-08431-1

Mohamed Khalith, S. B., Ramalingam, R., Karuppannan, S. K., Dowlath, M. J. H., Kumar, R., Vijayalakshmi, S., Uma Maheshwari, R., and Arunachalam, K. D. (2022). Synthesis and characterization of polyphenols functionalized graphitic hematite nanocomposite adsorbent from an agro waste and its application for removal of Cs from aqueous solution. *Chemosphere*, 286(P1),131493. https://doi.org/10.1016/j.chemosphere.2021.131493

Moutzouris, K., Papamichael, M., Betsis, S. C., Stavrakas, I., Hloupis, G., & Triantis, D. (2014). Refractive, dispersive and thermo-optic properties of twelve organic solvents in the visible and near-infrared. *Applied Physics B*, *116*, 617-622. https://doi.org/10.1007/s00340-013-5744-3

Muñiz-González, A. B. (2021). Ibuprofen as an emerging pollutant on non-target aquatic invertebrates: Effects on Chironomus riparius. *Environmental Toxicology and Pharmacology*, *81*, 103537. https://doi.org/10.1016/j.etap.2020.103537

Musah, M., Azeh, Y., Mathew, J. T., Umar, M. T., Abdulhamid, Z., & Muhammad, A. I. (2022). Adsorption kinetics and isotherm models: a review. *CaJoST*, *4*(1), 20-26.

N'diaye, A. D., & Kankou, M. S. A. (2020). Modeling of adsorption isotherms of pharmaceutical products onto various adsorbents: A Short Review. *J. Mater. Environ. Sci*, *11*(8), 1264-1276.

Nawaz, M., Wahab, Z., Rehman, Z.U., Bahader, A., Khan, M.I., Uddin, I., Gul, F.S. and Bajaber, M.A. (2023). Plant-mediated synthesis of iron oxide nanoparticles/polyvinyl alcohol nanocomposite and exploring their potential adsorption properties against selected heavy metals. *Polymer Bulletin*, 80(7), 7545-7567. https://doi.org/10.1007/s00289-022-04387-9

Ngernyen, Y., Petsri, D., Sribanthao, K., Kongpennit, K., Pinijnam, P., Pedsakul, R., & Hunt, A. J. (2023). Adsorption of the non-steroidal anti-inflammatory drug (ibuprofen) onto biochar and magnetic biochar prepared from chrysanthemum waste of the beverage industry. *RSC advances*, *13*(21), 14712-14728. DOI: 10.1039/D3RA01949G

DOI: 10.56892/bima.v8i4.1151

Nguyen, D.T.C., Le, H.T.N., Do, T.S., Pham, V.T., Lam Tran, D., Ho, V.T.T., Tran, T.V., Nguyen, D.C., Nguyen, T.D., Bach, L.G. and Ha, H.K.P. (2019). Metal-Organic Framework MIL-53 (Fe) as an Adsorbent for Ibuprofen Drug Removal from Aqueous Solutions: Response Surface Modeling and Optimization. *Journal of Chemistry*, *2*019(1), 5602957. https://doi.org/10.1155/2019/5602957

Osman, A. I., Ayati, A., Farghali, M., Krivoshapkin, P., Tanhaei, B., Karimi-Maleh, H., ... & Sillanpaä, M. (2024). Advanced adsorbents for ibuprofen removal from aquatic environments: a review. *Environmental Chemistry Letters*, *22*(1), 373-418. https://doi.org/10.1007/s10311-023-01647-6

Paul, D., Singhania, A., and Das, G. (2022). Catalytic activities of the vaterite and the calcite based solid supported catalysts for spontaneous Fenton-like dye degradation: A comparative study. *Journal of Environmental Chemical Engineering*, 10(3), 107558.

Plazinski, W., Dziuba, J., & Rudzinski, W. (2013). Modeling of sorption kinetics: the pseudo-second order equation and the sorbate intraparticle diffusivity. *Adsorption*, *19*, 1055-1064.

Priya, Naveen, Kaur, K., and Sidhu, A. K. (2021). Green synthesis: An eco-friendly route for the synthesis of iron oxide nanoparticles. *Frontiers in Nanotechnology*, *3*, 655062. https://doi.org/10.3389/fnano.2021.655062

Rafati, L., Ehrampoush, M. H., Rafati, A. A., Mokhtari, M., & Mahvi, A. H. (2018). Removal of ibuprofen from aqueous solution by functionalized strong nano-clay composite adsorbent: kinetic and equilibrium isotherm studies. *International journal of environmental science and technology*, *15*, 513-524. https://doi.org/10.1007/s13762-017-1393-0

Rata, D. M., Cadinoiu, A. N., Daraba, O. M., Gradinaru, L. M., Atanase, L. I., & Ichim, D. L. (2023). Influence of ZnO nanoparticles on the properties of ibuprofen-loaded alginate-based biocomposite hydrogels with potential antimicrobial and anti-inflammatory effects. *Pharmaceutics*, *15*(9), 2240. https://doi.org/10.3390/pharmaceutics15092240

Sadegh, H., Ali, G.A., Gupta, V.K., Makhlouf, A.S.H., Shahryari-Ghoshekandi, R., Nadagouda, M.N., Sillanpää, M. and Megiel, E. (2017). The role of nanomaterials as effective adsorbents and their applications in wastewater treatment. *Journal of Nanostructure in Chemistry*, *7*, 1-14. https://doi.org/10.1007/s40097-017-0219-4

Sandoval-González, A., Robles, I., Pineda-Arellano, C. A., and Martínez-Sánchez, C. (2022). Removal of anti-inflammatory drugs using activated carbon from agro-industrial origin: Current advances in kinetics, isotherms, and thermodynamic studies. *Journal of the Iranian Chemical Society*, 19(10), 4017-4033. https://doi.org/10.1007/s13738-022-02588-7

Sellaoui, L., Guedidi, H., Reinert, L., Knani, S., Duclaux, L., & Lamine, A. B. (2016). Experimental and theoretical studies of adsorption of ibuprofen on raw and two chemically modified activated carbons: new physicochemical interpretations. *RSC advances*, *6*(15), 12363-12373. https://doi.org/10.1039/C5RA22302D

DOI: 10.56892/bima.v8i4.1151

Shehata, M. G., Awad, T. S., Asker, D., El Sohaimy, S. A., Abd El-Aziz, N. M., and Youssef, M. M. (2021). Antioxidant and antimicrobial activities and UPLC-ESI-MS/MS polyphenolic profile of sweet orange peel extracts. *Current research in food science*, 4, 326-335. https://doi.org/10.1016/j.crfs.2021.05.001

Sherka, G. T., & Berry, H. D. (2024). Insight into impact of size and shape on optoelectronic properties of InX (X= As, Sb, and P) semiconductor nanoparticles: a theoretical study. *Frontiers in Physics*, *12*, 1447997. https://doi.org/10.3389/fphy.2024.1447997

Sithara, N. V., Bharathi, D., Lee, J., Mythili, R., Devanesan, S., & AlSalhi, M. S. (2024). Synthesis of iron oxide nanoparticles using orange fruit peel extract for efficient remediation of dye pollutant in wastewater. *Environmental Geochemistry and Health*, *46*(2), 30.

Sudhakar, C., Poonkothai, M., Selvankumar, T., and Selvam, K. (2022). Facile synthesis of iron oxide nanoparticles using Cassia auriculata flower extract and accessing their photocatalytic degradation and larvicidal effect. J. Mater. Sci. Mater. Electron. 33, 11434–11445. doi: 10.1007/s10854-022-08116-w

Trifoi, A. R., Matei, E., Râpă, M., Berbecaru, A. C., Panaitescu, C., Banu, I., & Doukeh, R. (2023). Coprecipitation nanoarchitectonics for the synthesis of magnetite: A review of mechanism and characterization. *Reaction Kinetics, Mechanisms and Catalysis*, *136*(6), 2835-2874.

Usman, O., Mohsin Baig, M. M., Ikram, M., Iqbal, T., Islam, S., Syed, W., ... & Naseem, M. (2024). Green synthesis of metal nanoparticles and study their anti-pathogenic properties against pathogens effect on plants and animals. *Scientific Reports*, *14*(1), 11354. https://doi.org/10.1038/s41598-024-61920-8

Vigdorowitsch, M., Pchelintsev, A., Tsygankova, L., & Tanygina, E. (2021). Freundlich isotherm: An adsorption model complete framework. *Applied Sciences*, *11*(17), 8078. https://doi.org/10.3390/app11178078

Vikram, S., Vasanthakumari, R., Tsuzuki, T., & Rangarajan, M. (2016). Investigations of suspension stability of iron oxide nanoparticles using time-resolved UV–visible spectroscopy. *Journal of Nanoparticle Research*, *18*, 1-24. https://doi.org/10.1007/s11051-016-3570-3

Yew, Y. P., Shameli, K., Miyake, M., Kuwano, N., Bt Ahmad Khairudin, N. B., Bt Mohamad, S. E., and Lee, K. X. (2016). Green synthesis of magnetite (Fe_3O_4) nanoparticles using seaweed (Kappaphycus alvarezii) extract. *Nanoscale research letters*, 11(1), 1-7. https://doi.org/10.1186/s11671-016-1498-2

Zubair, M., Saliq, Q., Manzar, M.S., Aziz, H.A., Haroon, H., Hung, Y.T., Wang, L.K. and Wang, M.H.S. (2023). Biochar for Adsorptive Removal of Pharmaceuticals from Environmental Water. In *Waste Treatment in the Biotechnology, Agricultural and Food Industries: Volume 2* (199-225). Cham: Springer International Publishing. https://doi.org/10.1007/978-3-031-44768-6_6.